

PDC: Piecewise Depth Completion utilizing Superpixels

Dennis Teutscher¹, Patrick Mangat¹ and Oliver Wasenmüller¹

Abstract—Depth completion from sparse LiDAR and high-resolution RGB data is one of the foundations for autonomous driving techniques. Current approaches often rely on CNN-based methods with several known drawbacks: flying pixel at depth discontinuities, overfitting to both a given data set as well as error metric, and many more. Thus, we propose our novel Piecewise Depth Completion (PDC), which works completely without deep learning. PDC segments the RGB image into superpixels corresponding the regions with similar depth value. Superpixels corresponding to same objects are gathered using a cost map. At the end, we receive detailed depth images with state of the art accuracy. In our evaluation, we can show both the influence of the individual proposed processing steps and the overall performance of our method on the challenging KITTI dataset.

I. INTRODUCTION

Currently, the transportation industry attaches great importance to the development of autonomous driving. Taking into account 3D Light Detection And Ranging (LiDAR) sensors becomes increasingly important. This sensor allows to determine sparse distance measurements at high accuracy. For further higher-level processing this sparse information needs to be transformed into a dense depth image. The method of creating a dense depth map from a sparse LiDAR input is called depth completion.

Recent approaches use different architectures of Convolutional Neural Networks (CNN) together with a high-resolution RGB image of the same scene for depth completion. Even though these methods are able to produce reasonable results, there are still some issues. The inference of depth values using convolutions creates so called flying pixels (see Figure 1 (e)) – especially in regions with discontinuities. Flying pixels are incorrect 3D points that connect a surface in the foreground to a surface in the background, even though there should be no geometry. Sometimes they are also called ghost points or slopes [1]. These flying pixels corrupt the depth image and yield an erroneous representation of reality. Additionally, CNN-based methods tend to be optimized for a particular data set and error metric, so generalization is sometimes not given.

To overcome these problems we introduce a novel geometry-based depth completion approach. The basic assumption of our method is that depth values on an object take similar values. Only at the transition between objects (e.g. foreground vs. background) larger discontinuities of depth values may occur. Therefore, one of the key tasks is to

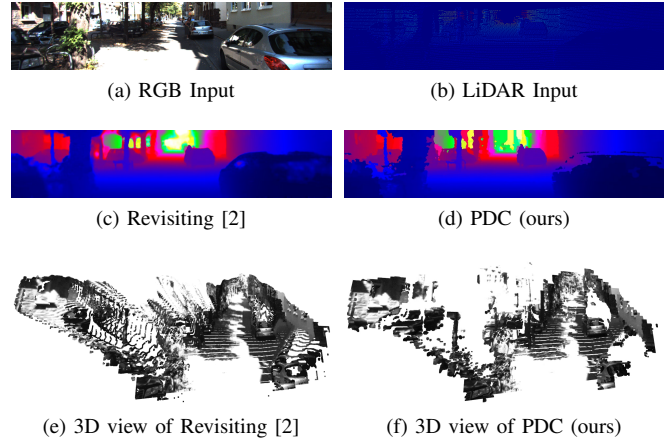


Fig. 1. We propose a novel piecewise depth completion (PDC) utilizing superpixels, which – in contrast to CNN-based methods [2] – effectively avoids the occurrence of flying pixels.

identify regions that are likely to have similar depth values. To do this, we subdivide the corresponding RGB image into superpixels. In order to find corresponding superpixels belonging to the same object, we use a cost map. Depth values can be interpolated within a cluster of associated superpixels. In our evaluation, we can show both the influence of the individual processing steps and the overall performance of our method. More depth maps and 3D views of our PDC can be found in Figure 7.

II. RELATED WORKS

Neural networks. Popular techniques for depth completion of sparse LiDAR inputs involve neural networks, which are able to learn the contours of objects and to approximate the corresponding depth values. Particularly suitable are Convolutional Neural Networks (CNNs) such as the sparsity-invariant CNNs [3] in the context of depth-only completion, relying on observable depth points only. In the so-called image guided depth completion the sparse depth is enriched by RGB images as additional input, allowing to infer additional information which is otherwise not accessible. For instance, in the method *Revisiting* [2] the depth completion with sparsity-invariant is assisted with RGB images as additional input. Further methods using RGB images are *Sparse to dense* [4], *DFuseNet* [5], *DFineNet* [6] and *Deep Lidar* [7]. Alternatively, one can combine RGB images and LiDAR input to train the CNNs for an interpolation approach of depth values. For example, based on these two inputs *MorphNet* [8] learns suitable morphological operations in order to complete the depth maps, while *NConv-CNN* [9] and

¹Mannheim University of Applied Sciences, Germany
dennis.teutscher@stud.hs-mannheim.de
p.mangat@hs-mannheim.de
o.wasenmuller@hs-mannheim.de

SSGP [10] learn the parameters of a regression model and for interpolation, respectively. Finally, the methods *Spade-sd* [11] and *ADNN* [12] both overcome sparsity as follows. The former uses a particular sparse training strategy while the latter employs techniques from compressed sensing.

Even though the CNN-based depth completion methods produce good results in many respects, they go along with various issues. First of all, those CNNs are typically trained on specific training data sets, which may not necessarily be sufficiently representative for their eventual application. Hence, when applying these trained CNNs to new data sets from different scenes, their performance often turns out to be less robust. Furthermore, these CNNs are usually trained with the goal of minimizing only a specific metric, which may not suffice to ensure a satisfactory overall result. For instance, one often chooses to minimize the root mean square error (RMSE). However, a simultaneous reduction of the mean absolute error (MAE) is not guaranteed. Finally, we want to emphasize the qualitative problem of flying pixels occurring in regions with discontinuities, induced by the convolutional layers and the approximation of depth values. This is a common problem of CNN-based methods, resulting in a manifestly erroneous depth image (see Figure 1 (e)).

Interpolation in flow estimation. Many fields of computer vision face the problem of dealing with sparse data sets. In particular, the problem of flow estimation shares similarities with the challenges we face in depth completion. Specifically, there are two well-known methods for optical flow estimation, namely *Epic Flow* [13] and *RIC-Flow* [14], which are based on interpolation of the matches without relying on neural networks. *RIC-Flow* does not use the raw matches directly but generate a superpixel flow from input matching to improve the efficiency of the model estimation. This concept was also adapted for scene flow estimation from sparse LiDAR and RGB image input [15]. Our approach, which we describe in detail in Section III, applies the superpixel method in the context of depth completion.

Depth completion without neural networks. To the best of our knowledge there is currently only one depth completion method on the KITTI benchmark [3], which does not use neural networks. This method is called *IP-Basic* [16], which uses traditional image processing operations to produce a dense depth map. It purely relies on the LiDAR input and hence avoids the potential risk of being optimized to some specific data sets only. In addition, *IP-basic* uses the Gaussian and the bilateral blur for additional refinements. By selecting a suitable filter this method also allows to control the problem of flying pixels. However, an open issue is that *IP-basic* yields an incorrect interpolation of sparse regions if there are objects in the near proximity. This problem will be discussed in more detail in IV-C.

Moreover, Buysens *et al.* [17] address the problem of inpainting occlusion holes in depth maps that occur when synthesizing virtual views of a RGB-D scene. Their solution is based on using superpixels to determine missing depth values in depth maps in the context of occlusion situations. However, since our use case is the depth completion on the

KITTI benchmark the results of our method are compared to *IP-basic*.

Own contributions. In this paper we develop a novel geometry-based depth completion method, where the depth maps are generated without the use of neural networks. Therefore, we automatically circumvent most of the previously mentioned problems of CNN-based methods. Our method makes use of the image processing operations of *IP-Basic* [16]. In order to overcome the problem of wrong interpolations of sparse regions we take inspiration from *RIC-Flow* [14] and introduce superpixels to geometry-based depth completion. We use superpixels in order to perform piecewise interpolation of the segments of the LiDAR input with similar depth values. Finally, the problem of flying pixels is solved by the choice of a suitable filter.

III. PROPOSED METHOD

In this section, we present our approach for the geometry-based piecewise depth completion (PDC) using superpixels. Given an RGB image as a reference and the sparse LiDAR input, our goal is to generate a dense depth map while avoiding the notorious problem of flying pixels known from CNN-based depth-completion methods. At the same time we want to produce results, which are qualitatively and quantitatively (based on RMSE and MAE) able to compete with the state of art methods of depth-completion. Our proposed method is summarized in Algorithm 1.

Algorithm 1 Summary of our algorithm PDC

- 1: Inverse LiDAR input
 - 2: Dilation LiDAR input
 - 3: Initialization $G(V, E)$
 - 4: Initialization $costmap$
 - 5: Initialization empty $mask$
 - 6: **for** s_i in V **do**
 - 7: **for** s_j with in $(s_i, s_j) \in E$ **do**
 - 8: Apply superpixel to $costmap$
 - 9: Compute $\epsilon(s_i, s_j)$
 - 10: **if** $\epsilon \leq \tau$ **then**
 - 11: Add s_j to shortlist L_i
 - 12: Compute cost $C(s_i, s_j)$ for $s_j \in L_i$
 - 13: **end if**
 - 14: **end for**
 - 15: Construct superpixel set from ranking L_i with respect to cost.
 - 16: Morphological close on superpixel set.
 - 17: Dilation on superpixel set.
 - 18: **for** s_j in superpixel set **do**
 - 19: Compute median of s_j
 - 20: Fill invalid values of s_j with median
 - 21: **end for**
 - 22: Copy superpixel set to $mask$
 - 23: **end for**
 - 24: Additional refinements
-

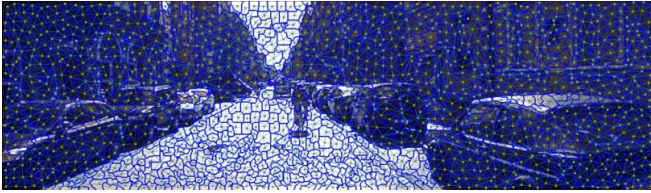


Fig. 2. We segment our image into superpixels, which give naturally rise to an undirected graph, where neighbors are connected by an edge. Upon using a suitable cost map it is then possible to identify the best fitting neighbors. This is the foundation for the interpolation of depth values within a set of associated superpixels.

A. Initialization

Our approach uses the given information of the LiDAR input as well as the image. In order to distinguish the depth values close to zero from invalid pixels, we invert the LiDAR input and subsequently use dilation to reduce its sparsity as proposed by Jason Ku *et al.* [16]. We assume that separate objects in the depth maps mostly consist of the same color but typically differ from the neighboring regions. Based on this assumption we segment the reference image into superpixels s_i using the segmentation method *SEED* [18].

Following [14], we introduce an undirected graph $G(V, E)$, where V is the set of all superpixels s_i and E is the set of edges (s_i, s_j) between neighboring superpixels s_i and s_j . An example of such a graph is shown in Figure 2. The Euclidean distance $D(s_i, s_j)$ of two neighboring superpixels s_i and s_j is given by

$$D(s_i, s_j) = \sqrt{(x_i - x_j)^2 + (y_i - y_j)^2}, \quad (1)$$

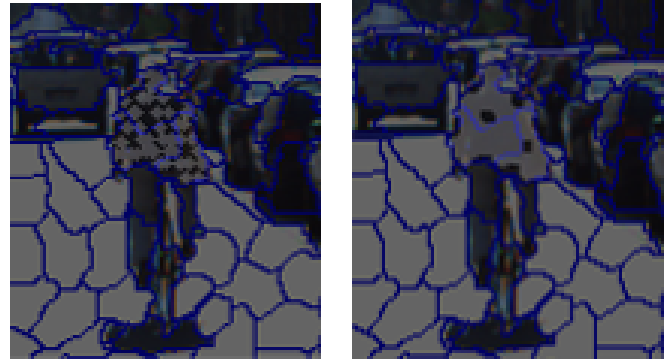
where (x_i, y_i) and (x_j, y_j) are the coordinates of the most centered pixels of superpixels s_i and s_j , respectively. The distance $D(s_i, s_j)$ will be used to penalize large distant superpixels.

The detection of the best fitting neighbor requires the use of cost maps. Y. Hu *et al.* [14] use the result of the structured edge detector SED [19] as their cost map. Alternatively, a cost map can be obtained from the reference image in gray scale. Since we already use the color information to segment the reference image it seems natural to also use the gray scale for the detection of the best fitting neighbors. Tests have shown that they produce similar results but the time consumption of the initialization of SED is significantly higher than the transformation to gray scale. These results can be found in Table II of Section IV. Consequently, we henceforth use the gray scale image to obtain the cost map.

B. Identification of the best fitting neighbors

A superpixel s_i can be interpreted as a cluster of many pixels. Each of those pixels obtains gray scale values, denoted by $v_k^{(i)}$, from the image. Given two neighboring superpixels s_i and s_j we compute the MAE (henceforce denoted by ϵ) for a sample of pixels as follows:

$$\epsilon(s_i, s_j) = \frac{1}{n} \sum_{k=1}^n |v_k^{(i)} - v_k^{(j)}| \quad (2)$$



(a) Inlier

(b) Morphological close



(c) Dilation

(d) Cut



(e) filling with median

Fig. 3. Our proposed method identifies the LiDAR inputs which belong to the same object (a). It uses a morphological close function to fill in the gaps (b), followed up by dilation in order to close small gaps (c). In the last step we cut out the set (d) and fill the remaining empty pixels with the median of the corresponding segment (e).

Here, n is the sample size defined by $n = \min(|s_i|, |s_j|)$, where $|s_i|$ denotes the number of pixels that make up superpixel s_i .

Based on $\epsilon(s_i, s_j)$ we construct a shortlist L_i of best fitting neighbors for s_i as follows: Any neighboring superpixel s_j is added to L_i if and only if $\epsilon(s_i, s_j) \leq \tau$, where $\tau > 0$ is some threshold. Now we rank these shortlisted superpixels according to some cost C , which disfavors large distant superpixels. Following [14] we define the cost C for s_j with respect to s_i by

$$C(s_i, s_j) = W \cdot \epsilon(s_i, s_j) \quad \forall s_j \in L_i, \quad (3)$$

where the weight function W is given by $W = \exp(-D(s_i, s_j)/\alpha)$ with some regularization parameter $\alpha > 0$. Therefore, each of the superpixels $s_j \in L_i$ has a corresponding cost $C(s_i, s_j)$. The two superpixels of L_i with the smallest cost are henceforth called the best fitting neighbors. The superpixels and their best fitting neighbors will be called superpixel set for the remainder of this paper.

C. Interpolation with morphological operations

Having constructed the superpixel sets we are able to cluster the pixels which possess similar depth values as seen in Figure 3 a). Therefore, we are in the position to make use of morphological operations for our interpolation approach.

We use the morphological close function to merge the pixels that are close to each other. However, large clusters of empty pixels are not filled by this step. To fill them, we use the dilated values of the superpixel set. Inserting the dilated values causes the pixels to go beyond the boundaries of our superpixel set as shown in Figure 3 (c). To fix this issue, the superpixels are cut out one by one along the boundaries. By doing this, we remove the overhanging pixels as illustrated in Figure 3 (d). At the same time we remove the depth values that were taken from the dilation from a neighboring superpixel. This ensures that if a neighbor was incorrectly declared an inlier, no incorrect depth data is transferred to other superpixels. Inspired by RIC-flow [14], the remaining empty pixels of this process are filled with the median of their respective superpixel as shown in Figure 3 (e). This iterative process is done for each superpixel set.

D. Additional refinements

Our approach only uses the existing depth values from the LiDAR input. However, larger objects may not be fully captured by the sensor, i.e. these objects are not fully covered by the depth map. To complete the depth map, the top row pixels are extrapolated to the top point of the image plane as is done in IP-Basic [16]. This step is optional and changes the result of the evaluation only insignificantly.

Furthermore, there can still be invalid pixels in the area covered by the sensor. This is a consequence of particularly sparse regions in the original LiDAR input. In order to fill the remaining invalid pixels, we follow the method of IP-basic [16] and overwrite the invalid pixels using dilated pixel values.

So far, our approach does not generate any flying pixels. However, this is no longer guaranteed once we further optimize the depth maps by including filters. The two relevant filters for this paper are the Gaussian blur and the bilateral blur. The former filter can be used to reduce the noise in our depth maps, but it does not have edge preserving properties. Hence, this filter will produce flying pixels in regions with an edge. In contrast, the bilateral blur does preserve edges. Therefore, our PDC method can be combined with a bilateral blur filter to further optimize the depth maps without running into the notorious problem of generating flying pixels.

TABLE I

WE COMPARE OUR PDC WITH DIFFERENT CONFIGURATIONS ON THE PUBLIC KITTI TRAINING DATA [3]. IT SHOWS THAT THE FORMATION OF SUPERPIXEL SETS POSITIVELY AFFECTS THE RESULTS.

bilateral blur	Gaussian blur	extrapolated	superpixel set	RMSE[mm]	MAE[mm]
X	X	X	✓	1426.163	313.368
X	X	✓	X	1429.664	294.238
X	X	✓	✓	1420.567	312.829
X	✓	X	X	1310.346	297.007
X	✓	X	✓	1307.856	295.152
X	✓	✓	X	1303.344	296.389
X	✓	✓	✓	1286.555	293.221
✓	X	X	X	1437.159	294.863
✓	X	X	✓	1434.791	293.312
✓	X	✓	X	1429.664	294.238
✓	X	✓	✓	1412.831	291.449

IV. EVALUATION

In this section, we show the design decisions of our PDC algorithm in a detailed ablation study. In addition, we perform a quantitative as well as qualitative evaluation on the KITTI dataset [3].

A. Ablation Study

One part of our contribution is the search of the best possible neighbors for our interpolation (see Section III-B). In order to show that this step has a significant positive impact on the evaluation results, we present in Table I the results of our method with and without the use of a superpixel set where each superpixel is interpolated separately. We also show the results of the two filters as well as with and without extrapolation (see Section III-D) of the pixels to the top of the frame. This evaluation shows that the interpolation with a superpixel set generates consistently better results with regard to RMSE and MAE.

We can observe that the Gaussian blur achieves the best RMSE, but the bilateral blur achieves the best MAE. The reason for this is that the RMSE accounts for larger errors in the depth map more than the MAE. The conclusion is that the Gaussian blur is able to reduce the noise of larger flat regions more efficiently than the bilateral blur, while it gives a worse result in edge regions that can be considered as small errors. From this evaluation, we can conclude that the bilateral blur is the more suitable filter because it preserves more precise contours of objects.

In addition, we compare the time required to initialize the cost maps (see section III-A) for a depth map in Table II. It can be seen that although the error metrics are almost the same, the time required by SED [19] is significantly higher.

It is important to note that we have not yet focused our PDC on optimizing the computation time but on the quality of the depth maps. Currently, the computational step of finding each superpixel and its neighbors is computationally very intensive. The optimization of the computational time is left for future work.

B. Quantitative Evaluation

The best method so far on the KITTI dataset, which also does not use deep learning, is the IP-Basic [16] approach. In

TABLE II

WE COMPARE THE RESULTS OF THE TWO COST MAPS. IT SHOWS THAT THE GRAY SCALE IMAGE ACHIEVES SIMILAR RESULTS TO SED BUT INITIALIZES MUCH FASTER. FOR THIS RESULT THE FOLLOWING ENVIRONMENT WAS USED: 1 CORE @3.6GHZ (PYTHON).

	RMSE [mm]	MAE [mm]	extra time per image [s]
SED [19]	1286.536	293.259	1.38688
gray scale image	1286.555	293.221	0.0109

TABLE III

WE COMPARE IP-BASIC [16] WITH PDC (OURS) ON THE PUBLIC KITTI TRAINING DATA [3]. IT CAN BE SEEN THAT PDC (OURS) WITH THE FILTERS USED BY IP-BASIC, PRODUCES BETTER RESULTS OVERALL.

	RMSE[mm]		MAE[mm]	
	Gaussian blur	Bilateral blur	Gaussian blur	Bilateral blur
IP-Basic [16]	1350.927	1454.754	305.352	303.699
PDC (ours)	1286.555	1412.831	293.221	291.449

Table III, we compare our new PDC against this approach. It turns out that our method, with the additional use of an RGB image instead of just using the raw LiDAR data as input, consistently yields better results. The error metrics show that the Gaussian blur produces the better RMSE while the bilateral blur produces the better MAE.

For the purpose of comparing our method quantitatively with the state of art, we submitted our results on the KITTI benchmark test [3]. We present the evaluation result in Table IV which we structure as follows. The CNN column describes if the pictured method uses a convolution neural network, the RGB column depicts if an RGB image is additionally used for guided depth completion and learning interpolation is used to describe if a method learns parameters to interpolate the depth values.

This evaluation shows that our method achieves similar results on the public and anonymous KITTI datasets [3]. Therefore we do not have the problem of optimization and our approach is robust with different inputs. While the best CNN based methods yield better results in respect to the RMSE, our proposed method is en par regarding the MAE. Deep learning optimizes the RMSE and neglects the MAE. Therefore, the MAE is proportionally better with ours. The same is true for IP-Basic [16]. Consequently, this observation supports our investigation into geometry-based approach to depth completion as a competitor to established deep-learning methods.

C. Qualitative Evaluation

IP-Basic vs. PDC (ours). In order to show that our approach handles the interpolation of sparse regions better than IP-Basic [16] we visually compare it with PDC in Figure 4. It shows that in areas close to invalid pixels IP-Basic struggles to keep the contours of the objects.

These problems arise because IP-Basic does not differentiate between objects. Furthermore, it uses the pixels from the car to fill the gaps in the wall close to it. Our PDC does not have these problems because we use a piecewise

TABLE IV

WE COMPARE OUR METHOD WITH THE STATE OF THE ART FROM THE KITTI BENCHMARK [3]. IT SHOWS THAT PDC (OURS) DOES NOT PERFORM AS WELL AS CNN-BASED METHODS IN TERMS OF RMSE, BUT CAN COMPETE WITH THEM IN TERMS OF MAE.

	CNN	RGB	learning interpolation	RMSE[mm]	MAE[mm]
Deep Lidar [7]	✓	✓	✗	758.38	226.50
Revisiting [2]	✓	✓	✗	792.80	225.81
Sparse to Dense [4]	✓	✓	✗	814.73	249.95
SSGP [10]	✓	✓	✓	838.22	244.7
DFineNet [6]	✓	✓	✗	943.89	304.17
Spade-sD [11]	✓	✓(✗)	✗	1035.29	248.32
MorphNet [8]	✓	✓	✓	1045.45	310.49
DFuseNet [5]	✓	✓	✗	1206.66	429.93
PDC(ours)	✗	✓	✗	1227.96	288.55
NConv-CNN [9]	✓	✓	✗	1268.22	360.28
IP-Basic [16]	✗	✗	✗	1288.46	302.60
ADNN [12]	✓	✗	✗	1325.37	439.48
NN+CNN [3]	✓	✗	✗	1419.75	416.14
SparseConvs [3]	✓	✗	✗	1601.33	481.27

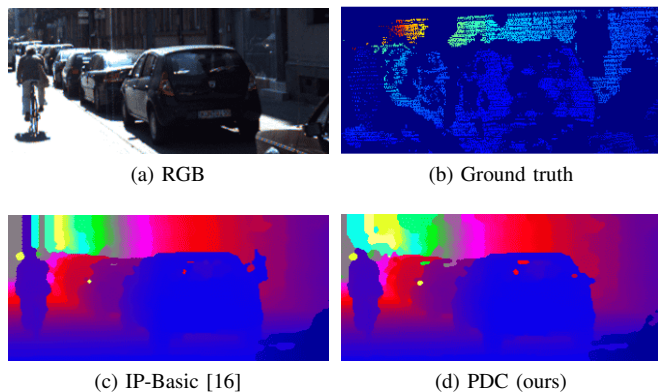


Fig. 4. This figure shows that PDC (d) is able to produce a reliable result even in sparse regions, while IP-Basic (c) does not. The ground truth (b) shows that the wrong interpolation do not get evaluated.

interpolation approach where the used data is usually from the same object. Since there is no ground truth at these regions it does not impact the metric based evaluation even though a significant error in the depth map is visible. Thus, we were also able to show visually that our method produces significantly higher quality depth information than IP-Basic.

CNN based vs. PDC (ours). The CNN-based method Revisiting [2] uses SI-Convolution and an RGB image as additional input. The method produces good results in terms of RMSE and MAE. Since it can compete with the best methods on the KITTI benchmark [3], we use it as the representative CNN-based method. So in order to further support our claim that our method is able to compete with CNN-based methods, we compare the resulting depth maps of Revisiting [2] with ours. For this purpose, we decided to select a representative image with a potential danger for a pedestrian and consider the depth map of this said person in Figure 5.

It shows that PDC is able to preserve the edges of the person and can be recognized in the depth map as such. In the depth map of Revisiting it is harder to recognize the person since she melts together with the car which makes

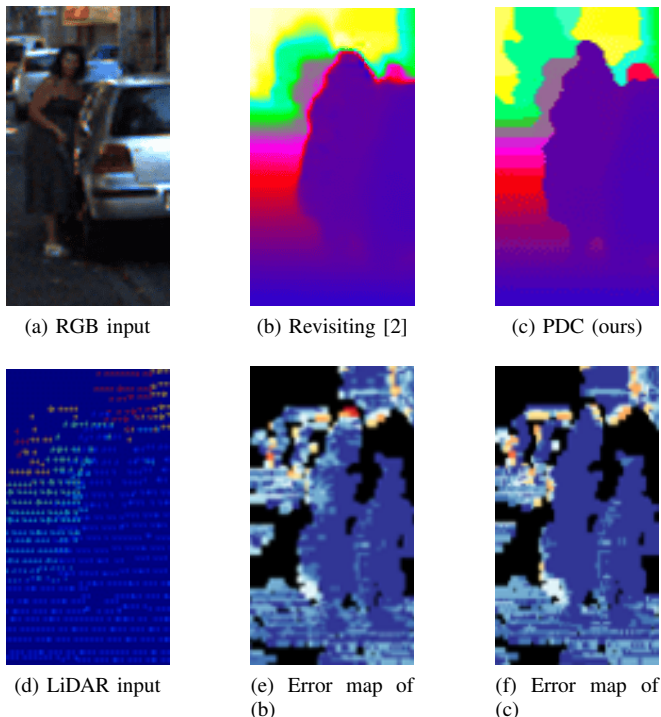


Fig. 5. This figure shows the resulting depth maps (c) and (d) from the LiDAR input (b). In the corresponding error maps (e) and (f) the blue pixels are the correct estimated depth values.

it harder to differentiate. The error maps in Figure 5 (e) and Figure 5 (f) makes this more apparent and show how the approximation of the depth values do not reflect the reality. Since our approach only uses the present data and does not approximate we have more depth values in the error map which correspond to the ground truth. We have noticed that our approach is not able to compete with CNN based methods in regions with exceptionally sparse LiDAR input but our method is a strong contender in regions with dense input. Since most of the dense areas are right in front of the car in a close proximity it is obvious that these are very important regions. This comparison was done with all listed CNN based methods from Table IV with similar results.

The other issue is the flying pixels which are often generated by CNN based methods. The depth map from Revisiting (see Figure 5 (b)) shows that there are red pixels around the pedestrian. That means that they are farther away from the person and do not represent the reality. This corresponds to a transition of pixels, which are then visible as flying pixels in the 3D view. Usually they are not considered in the evaluation because there are often no ground truths in this edge regions. This can be observed in the error maps in Figure 5 (e) and Figure 5 (f) where the black spots represent the absence of the ground truth values. In Figure 6 these flying pixels are visualized for this specific example and show that the pedestrian in Figure 6 (a) is completely distorted while it is not true for the results of our method in Figure 6 (b). The whole depth map and the 3D view from which this detail is taken is shown in the Figure 1.

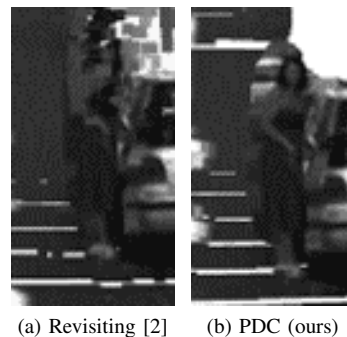


Fig. 6. 3D view of the depth map from Figure 5 which shows how the flying pixels distort the pedestrian in (a) in comparison with PDC (ours) (b) where no distortion takes place

V. CONCLUSION

In this paper, we have introduced a new geometry-based approach for depth completion by using superpixels for a piecewise interpolation of the depth map. We show that we can produce reliable depth maps with the segmentation of an additional RGB image into superpixels. The identification of suitable interpolation partners sharing similar depth values eliminates the problem of erroneous interpolation in sparse regions. We have also shown that our PDC avoids flying pixels as well as can compete with and outperform CNN-based depth completion methods in some regions.

ACKNOWLEDGMENT

This work was funded by the Karl Völker Foundation in the project "KI-Fusion". We thank Laurenz Reichardt for the fruitful discussions and his positive inputs.

REFERENCES

- [1] O. Wasenmüller, G. Bleser, and D. Stricker, "Combined bilateral filter for enhanced real-time upsampling of depth images," in *International Conference on Computer Vision Theory and Applications (VISAPP)*, 2015.
- [2] L. Yan, K. Liu, and E. Belyaev, "Revisiting sparsity invariant convolution: A network for image guided depth completion," *IEEE Access*, 2020.
- [3] J. Uhrig, N. Schneider, L. Schneider, U. Franke, T. Brox, and A. Geiger, "Sparsity invariant cnns," in *International Conference on 3D Vision (3DV)*, 2017.
- [4] F. Ma, G. V. Cavalheiro, and S. Karaman, "Self-supervised sparse-to-dense: Self-supervised depth completion from lidar and monocular camera," in *International Conference on Robotics and Automation (ICRA)*, 2019.
- [5] S. S. Shivakumar, T. Nguyen, I. D. Miller, S. W. Chen, V. Kumar, and C. J. Taylor, "Dfusenet: Deep fusion of rgb and sparse depth information for image guided dense depth completion," in *IEEE Intelligent Transportation Systems Conference (ITSC)*, 2019.
- [6] Y. Zhang, T. Nguyen, I. D. Miller, S. S. Shivakumar, S. W. Chen, C. J. Taylor, and V. Kumar, "Dfinenet: Ego-motion estimation and depth refinement from sparse, noisy depth input with rgb guidance," *Computing Research Repository (CoRR)*, 2019.
- [7] J. Qiu, Z. Cui, Y. Zhang, X. Zhang, S. Liu, B. Zeng, and M. Pollefeys, "DeepLidar: Deep surface normal guided depth prediction for outdoor scene from sparse lidar data and single color image," in *IEEE Conference on Computer Vision and Pattern Recognition (CVPR)*, 2019.
- [8] M. Dimitrievski, P. Veelaert, and W. Philips, "Learning morphological operators for depth completion," in *Advanced Concepts for Intelligent Vision Systems (Acicvs)*, 2018.

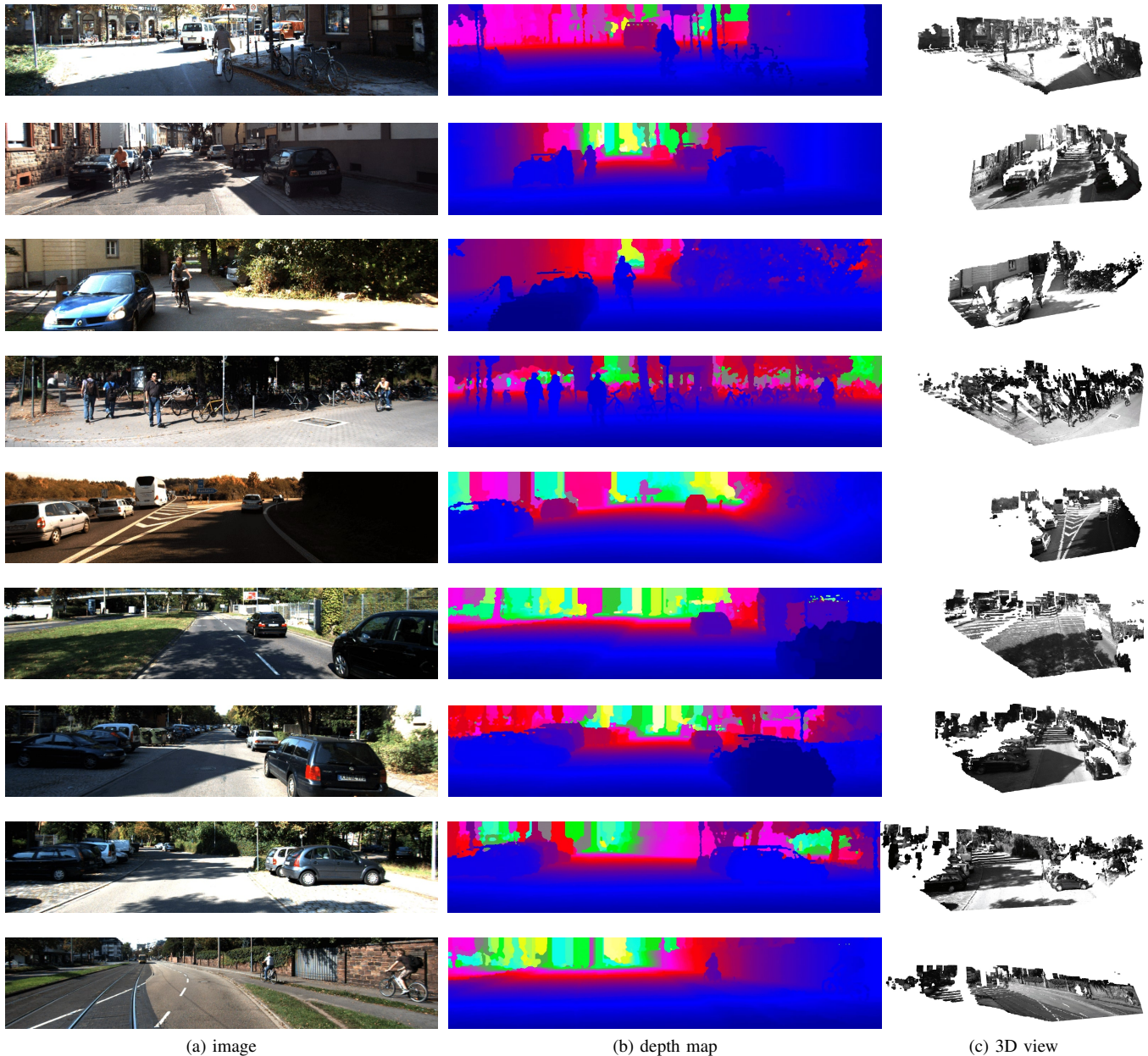


Fig. 7. We display the resulting depth maps from our PDC for several examples. The row with the 3D views show that no flying pixels are generated.

- [9] A. Eldesokey, M. Felsberg, and F. S. Khan, "Propagating confidences through cnns for sparse data regression," *Computing Research Repository (CoRR)*, 2018.
- [10] R. Schuster, O. Wasenmüller, C. Unger, and D. Stricker, "Ssgp: Sparse spatial guided propagation for robust and generic interpolation," in *IEEE Winter Conference on Applications of Computer Vision (WACV)*, 2021.
- [11] M. Jaritz, R. D. Charette, E. Wirbel, X. Perrotton, and F. Nashashibi, "Sparse and dense data with cnns: Depth completion and semantic segmentation," in *International Conference on 3D Vision (3DV)*, 2018.
- [12] S. L. Nathaniel Chodosh, Chaoyang Wang, "Deep Convolutional Compressed Sensing for LiDAR Depth Completion," in *Asian Conference on Computer Vision (ACCV)*, 2018.
- [13] J. Revaud, P. Weinzaepfel, Z. Harchaoui, and C. Schmid, "Epicflow: Edge-preserving interpolation of correspondences for optical flow," in *IEEE Conference on Computer Vision and Pattern Recognition (CVPR)*, 2015.
- [14] Y. Hu, Y. Li, and R. Song, "Robust interpolation of correspondences for large displacement optical flow," in *IEEE Conference on Computer Vision and Pattern Recognition (CVPR)*, 2017.
- [15] R. Batraway, R. Schuster, O. Wasenmüller, Q. Rao, and D. Stricker, "Lidar-flow: Dense scene flow estimation from sparse lidar and stereo images," in *IEEE/RSJ International Conference on Intelligent Robots and Systems (IROS)*, 2019.
- [16] J. Ku, A. Harakeh, and S. L. Waslander, "In defense of classical image processing: Fast depth completion on the cpu," in *Conference on Computer and Robot Vision (CRV)*, 2018.
- [17] P. Buysens, M. Daisy, D. Tschumperlé, and O. Lézoray, "Superpixel-based depth map inpainting for rgb-d view synthesis," in *IEEE International Conference on Image Processing (ICIP)*, 2015.
- [18] M. Van den Bergh, X. Boix, G. Roig, B. Capitani, and L. Van Gool, "Seeds: Superpixels extracted via energy-driven sampling," in *International Journal of Computer Vision (IJCV)*, 2012.
- [19] P. Dollár and C. Zitnick, "Fast edge detection using structured forests," *IEEE Transactions on Pattern Analysis and Machine Intelligence (TPAMI)*, vol. 37, 2014.